Rafael Kenji Nishihora, Laura Luhede, Udo Fritsching, Mara Gabriela Novy Quadri, Dachamir Hotza, Kurosch Rezwan, Michaela Wilhelm

Premix membrane emulsification using flat microfiltration inorganic membranes with tailored structure and composition

Rafael Kenji Nishihora, Laura Luhede, Udo Fritsching, Mara Gabriela Novy Quadri, Dachamir Hotza, Kurosch Rezwan, Michaela Wilhelm, Premix membrane emulsification using flat microfiltration inorganic membranes with tailored structure and composition, Journal of Membrane Science, Volume 608, 2020, 118124, ISSN 0376-7388, https://doi.org/10.1016/j.memsci.2020.118124.

Premix membrane emulsification using flat microfiltration inorganic membranes with tailored structure and composition

Rafael Kenji Nishihora [a,b], Laura Luhede [c], Udo Fritsching [c,d], Mara Gabriela Novy Quadri [b], Dachamir Hotza [b], Kurosch Rezwan [a,d], Michaela Wilhelm [a,*]

[a] University of Bremen, Advanced Ceramics, Am Biologischen Garten 2, IW3, D-28359, Bremen, Germany
[b] Department of Chemical Engineering and Food Engineering (EQA), Federal University of Santa Catarina (UFSC), 88040-900, Florianópolis, SC, Brazil
[c] Leibniz-Institute for Materials Engineering IWT, Department of Particles and Process Engineering, University of Bremen, Badgasteiner Str. 3, D-28359, Bremen, Germany
[d] MAPEX Center for Materials and Processes, University of Bremen, 28359, Bremen, Germany

Keywords:
Premix membrane emulsification
Ceramic membranes
Asymmetric structure
Symmetric structure
Oil-in-water emulsions

A B S T R A C T

Uniform oil-in-water emulsions were prepared using MCT (medium-chain fatty acid triglyceride, 10 wt%) as the oily dispersed phase and polysorbate 80 as the surfactant (1 wt%). The emulsification process was performed via premix membrane emulsification (PME) using 3 flat microfiltration ceramic membranes with different mean pore sizes (d_m): borosilicate (symmetric, commercial, d_m: 1.39 μm); SiOC (symmetric, manufactured, d_m: 1.76 μm); and mullite (asymmetric, manufactured, d_m: 1.18 μm). The droplets size and their distribution varied according to the membrane type and number of permeation cycles (up to a limit of 2 passes). All prepared emulsions presented a tendency to monomodal droplet distribution with span values in the range of 0.82–0.97. The coarse emulsion (premix) droplets were reduced from 6.30 to 4.50–2.17 μm. The asymmetric membrane (mullite) exhibited the highest permeation fluxes at constant relative pressure for both water (43.1×10^{-3} m^3 m^{-2} s^{-1}) and premix (Pass 1: 4.6×10^{-3} m^3 m^{-2} s^{-1}; Pass 2: 5.3×10^{-3} m^3 m^{-2} s^{-1}), still maintaining satisfactory emulsification results.

1. Introduction

A simple emulsion system consists of a mixture of two immiscible liquid phases. The major component of such a mixture is called the continuous phase, and the minor one is the dispersed phase [1]. Emulsions play an important role in cosmetics, pharmaceuticals, paints, as well as in chemicals, petrochemical, and food products [2,3]. Even though there are plenty of techniques already established in the lab and industrial scale to prepare emulsified systems, they still present some technological issues. For instance, conventional emulsification devices, such as colloid mills and dispersing machines consume low energy but produce polydispersed emulsions. On the other hand, high-pressure homogenizers generate monodispersed emulsions at the expense of high-energy consumption [3–5]. To overcome the operational limitations from the aforementioned devices, the technology of membrane emulsification (ME) has been attracting great attention as a sustainable and efficient alternative [6,7].

The primary features of membrane emulsification include: (i) production of uniform droplets with a narrow size distribution, (ii) low shear stress, (iii) low energy requirement, (iv) tailoring of droplet size by the proper selection of the membrane, and (v) operational flexibility and simplicity [8].

There are two main ME processes: direct or cross-flow, and premix membrane emulsification (PME). In the direct membrane emulsification (DME), an applied pressure forces the to-be-dispersed phase through the porous structure of a membrane into the cross-flowing continuous phase, which can contain stabilizers (e.g. surfactants) [9,10]. The PME method starts already with a coarse emulsion, which is pushed through a membrane to produce a finer emulsion [11]. The PME process main advantages are the droplet uniformity at higher fluxes ($>2.78 \times 10^{-4}$ m^3 m^{-2} s^{-1}), smaller mean droplet sizes, simpler experimental set-up, and easier process control [12]. One of the major disadvantages in PME is the polydispersity compared to DME, which normally can be overcome by increasing the number of cycles or passes through the membrane [13]. However, the membrane characteristics is noteworthy the primary key component in these processes.

* Corresponding author.
E-mail address: mwilhelm@uni-bremen.de (M. Wilhelm).

Table 1
Main characteristics of the applied inorganic membranes.

Membrane	Average pore size (μm)	Thickness (μm)	Composition	Reference
Por2 (Support)	40–100	1000	Borosilicate Glass (symmetric structure)	[18,19]
Por4 (Premix production)	10–16	3500		[18,19]
Por5	1–1.6	1000		[18,19]
SiOC	1.76	1000	Silicon OxyCarbide (symmetric structure)	[21]
Mullite	1.2[a]	6.11[a]	Mullite (asymmetric structure)	[20]

The Por"x" membranes are commercially available products.
[a] Value related to the top layer of the asymmetric Mullite membrane.

Several parameters are involved in PME process; however, the literature emphasizes especially the transmembrane pressure, disperse phase fraction, stabilizers, continuous phase viscosity, number of homogenizing cycles, and membrane properties [11]. Among membrane properties, the pore size (and distribution), porosity, interconnectivity, surface properties, and material class (polymeric, metallic, or ceramic) should be highlighted [6]. There is an increasing interest in applying ceramic membranes as an alternative to the conventional metallic sieves and polymeric membranes. This is mainly due to the chemical and structural stability intrinsic to ceramic materials [14]. Most of the efforts regarding the use of ceramic membranes in ME processes involve the so-called Shirasu Porous Glass (SPG) membranes, due to their narrow pore size range [15,16].

Therefore, this work aims to address the lack of research studies on the application of a larger variety of inorganic membranes in the ME process. With this in mind, we present a systematic investigation evaluating the feasibility of producing oil-in-water emulsions by PME, using three distinct microfiltration flat ceramic membranes. The influence of process parameters on the mean droplet size, size distribution, and permeation flux are evaluated and compared to the main studies concerning PME of oil-in-water emulsions using glass and ceramic membranes in a dead-end configuration.

2. Experimental

2.1. Chemicals and membranes

The emulsions were prepared based on previous work from the group [17] with a medium-chain triglycerides oil (MCT, viscosity = 290 mPa s at 200 s^{-1} and 20°C, density = 952 kg m^{-3}, refractive index = 1.450) as dispersed phase. A non-ionic surfactant was added to the continuous aqueous phase (polysorbate 80, Tween® 80, Sigma-Aldrich). Concerning the inorganic membranes employed in this work, their main characteristics are summarized in Table 1. In order to prepare a stable premix, a commercially available sintered-glass membrane was used (Por4, Robu Glasfilter-Geräte) with pore size of 10–16 μm, according to ISO 4793–80 (Fig.S1) [18,19]. For the premix emulsification tests, three flat ceramic membranes with 10 mm of diameter and ~1.0 mm of thickness were studied. However, the effective selective layer (top/-skin-layer) of the asymmetric mullite membrane has a thickness of 6.11 μm [20]. The commercially available membranes (Por2, Por4, and Por5, Robu Glasfilter-Geräte) consist of a symmetric structure made of sintered non-spherical fragmented borosilicate glass (80.6% SiO_2, 12.6% B_2O_3, 4.2% Na_2O, 2.2% Al_2O_3, 0.29% others, by weight). According to the supplier, Por5 presents a pore size in the range of 1–1.6 μm (ISO 4793–80) [18,19]. The other two membranes, the symmetric SiOC and the asymmetric mullite have been prepared, further described and characterized in previous studies [20,21], in which they are referred to as "SiC6.5-A30-1000" and "Diac-1200-1650", respectively. The support

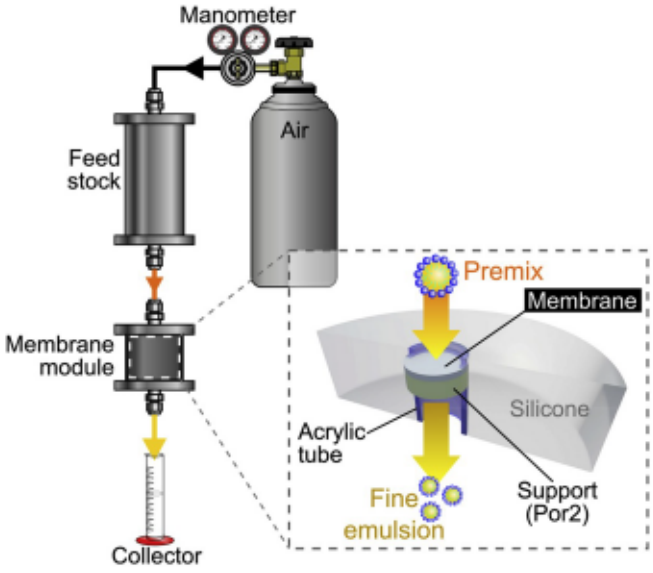

Fig. 1. Schematic representation of the premix membrane emulsification setup (adapted from Ref. [20]).

structure (Por2, Robus Glasfilter-Geräte, as indicated in Fig. 1) presents a coarse pore size distribution (40–100 μm, ISO 4793–80; Fig.S1) [19] and has the same composition as Por4 and Por5. Preliminary tests showed that the support (Por2) has no influence on the permeation and emulsification experiments (see Fig. S2).

2.2. Premix preparation

The premix was prepared by mixing 1 wt% polysorbate 80 in 89 wt% bidistilled water for 2 min in a magnetic stirrer (200 rpm, ~25 °C). Then, 10 wt% MCT oil was added and dispersed by a rotor-stator device (IKAs T18 basic Ultraturrax), applying a constant rotation speed of 3600 min^{-1} for 30 s. Subsequently, the obtained mixture was passed once through the Por4 glass membrane at 6 bar using the setup displayed in Fig. 1 to produce a less unstable coarse premix.

2.3. Membrane permeation flux and premix emulsification tests

For the water permeation and premix emulsification experiments, a testing flow-through-membrane disc device was used as schematically shown in Fig. 1. The silicone ring for fixing the membrane displayed in Fig. 1 was prepared using a commercial silicone elastomer (Sylgard® 184, Dow Corning), which successfully provided the side sealing of the membrane. Due to mechanical and flux constraints observed during experimental tests, all the experiments comparing the three membranes were performed at a fixed pressure of 5 bar. The permeation flux was calculated according to the following equation:

$$J = \frac{1}{A}\frac{dV}{dt} \quad (1)$$

where J is the membrane permeation flux ($m^3\ m^{-2}\ s^{-1}$); A is the effective transverse area of the membrane (m^2); dV and dt represent the variation in permeated volume (m^3) and time (s), respectively.

For the emulsification tests, the collected permeated premix was forced through the membranes for two times (without cleaning in between), after which no further changes on droplet size could be observed for our system.

2.4. Membrane and emulsion characterisation

The morphology of the membranes was analyzed by scanning

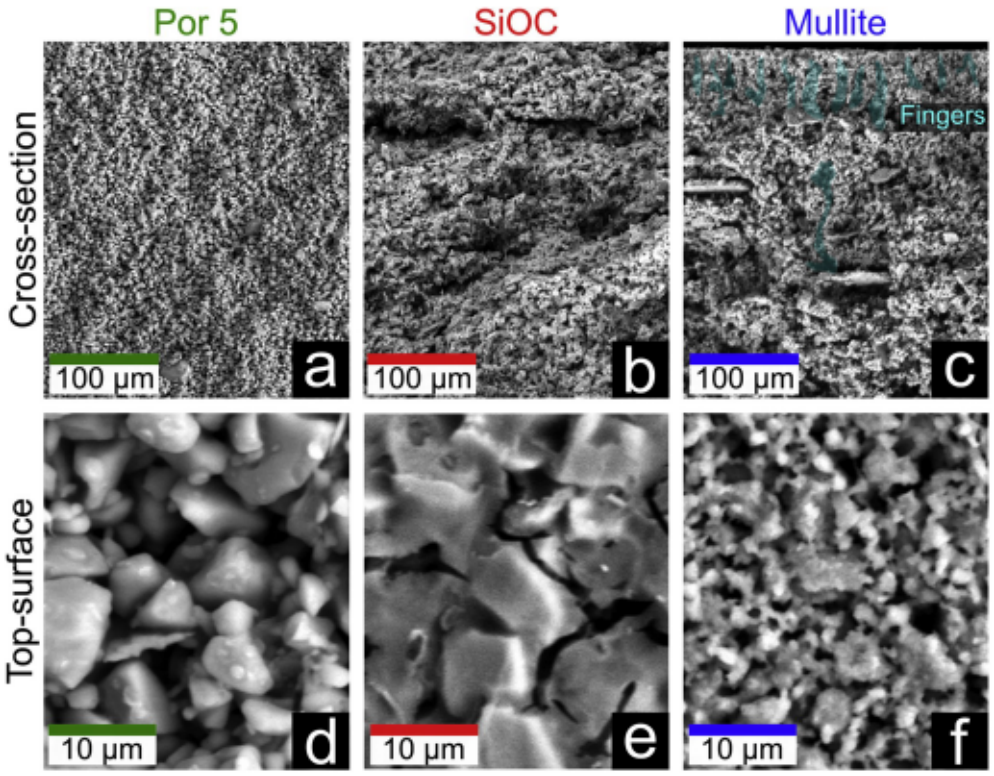

Fig. 2. Cross-section and top surface SEM images of the symmetric membranes (a,d) Por5 and (b,e) SiOC (the image presented in "b" was adapted from Ref. [21]), and the asymmetric mullite membrane (c,f).

electron microscopy (SEM, 20 kV, Series 2, Obducat CamScan). For this purpose, the samples were sputtered with gold (K550 Emitech Judges Scientific). Porosity and pore size distribution of the membranes were determined using mercury intrusion porosimetry (Pascal 140/440, Porotec). Due to the asymmetric morphology of the mullite membrane, the SEM surface micrograph of the top layer was examined by image analysis (ImageJ software). Hydrophobicity and hydrophilicity were investigated by measuring water and n-heptane vapor adsorption based on the method described in previous works from the group [21,22].

The droplet size and distribution of the emulsions and premix were measured by a laser particle size analyzer (Horiba LA-960). The continuous phase was distilled water with a refractive index of 1.333. The droplet size distributions are characterized by the mean droplet size expressed in terms of the median diameter ($d_{50,3}$) and the width of the distribution is given by the span value defined as:

$$span = \frac{d_{90,3} - d_{10,3}}{d_{50,3}} \quad (2)$$

where d_x is the diameter corresponding to x value on a relative cumulative droplet size distribution curve. All measurements were done in triplicate; the values reported are the average of three measurements.

3. Results and discussion

3.1. Membrane characteristics

The morphology of the cross-section and top surface of the ceramic membranes are depicted in Fig. 2. The commercial membrane Por5 exhibits a homogeneous inner microstructure (Fig. 2a) with irregular pore shapes due to the non-spherical fragmented borosilicate glass (Fig. 2d) that composes its structure. The SiOC membrane seems to present an uniform distribution of irregular rounded pores accompanied by some cracks in the cross-section (Fig. 2b). On the other hand, the top surface displays irregular pores mostly in a crack-like shape (Fig. 2e), probably as a result of the gas release during pyrolysis [23]. The asymmetric mullite membrane (see Fig. 2c) consists of a top-layer with a thickness around 6 µm followed by a support layer that is composed of a small portion of a finger-like structure (highlighted in light blue) and majorly a sponge-like layer. The top surface (Fig. 2f) shows regions with more homogeneous pore distributions in which a mix of spherical and irregular shapes is present. Nevertheless, a few large pores are also observed, mostly with irregular pore shapes.

Fig. 3a displays the pore diameter distribution (µm) and open porosity (%) of the studied membranes. All analyzed samples show a pore diameter on the microfiltration range (0.1–5 µm). The Hg-intrusion analysis of the symmetric membranes reveals a similar mean pore size (d_m), in which Por5 exhibits the smallest value of 1.39 µm while SiOC has 1.76 µm. Despite the mentioned similarity, Por5 presents the narrowest distribution and more than the double of open porosity (77.83%) when compared to the SiOC membrane (36.45%). The mullite asymmetric membrane presents the highest mean pore size (3.06 µm), the widest distribution, and a considerable open porosity (68.27%). These results reflect the great variation in the pore structure visualized in the support layer of the mullite membrane (Fig. 2c). Nevertheless, when analyzing the top surface (skin-layer) of this asymmetric membrane (Fig. 3b), the pore size range (1.2 ± 0.8 µm) is comparable to the main peaks exhibited by the other two membranes.

The surface characteristics (hydrophilicity-hydrophobicity) of the membranes were accessed by the vapor adsorption of a non-polar (n-heptane) and a polar (water) solvent (Fig. 4). Despite the differences in the magnitude of water and n-heptane uptake (mmol m^{-2}), all membranes are hydrophilic (ratio > 1). The hydrophilic nature is inherent to the oxide ceramic materials [24]. Unexpectedly, the SiOC membranes present the most elevated water by n-heptane ratio (5.84) among the tested membranes (Por5 = 4.37; mullite = 1.60). Notwithstanding the presence of carbon and SiC domains in their structure, the hydrophilicity is presumed to be due to the hydrophilic amorphous SiO_2-rich nanodomains that are accessed by the water vapor molecules [25,26].

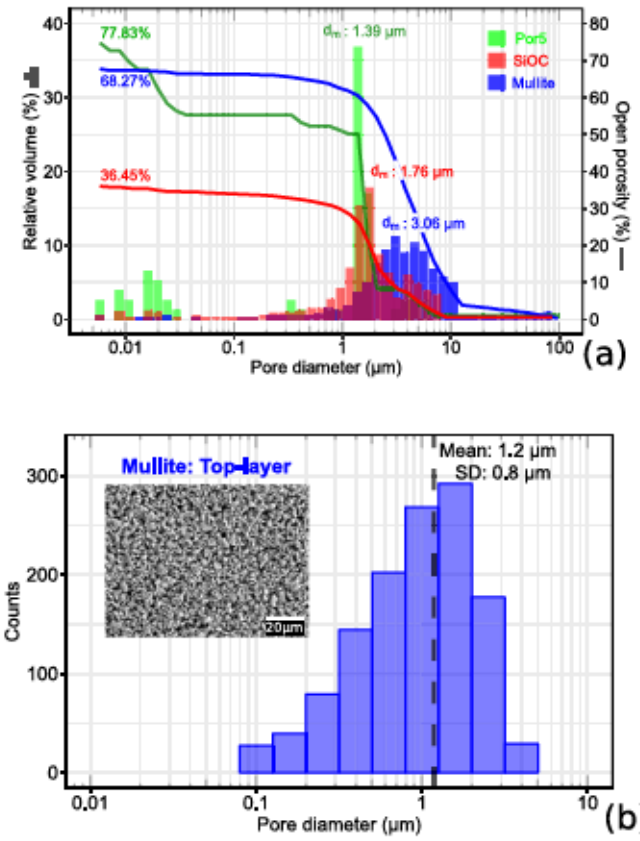

Fig. 3. (a) Pore size distribution versus relative pore volume (bars) and open porosity curves (lines) measured by Hg-porosimetry (the data referred to SiOC and mullite were adapted from Ref. [20,21], respectively). (b) Pore size distribution of the skin-layer of the mullite asymmetric membrane obtained from SEM image analysis (ImageJ software).

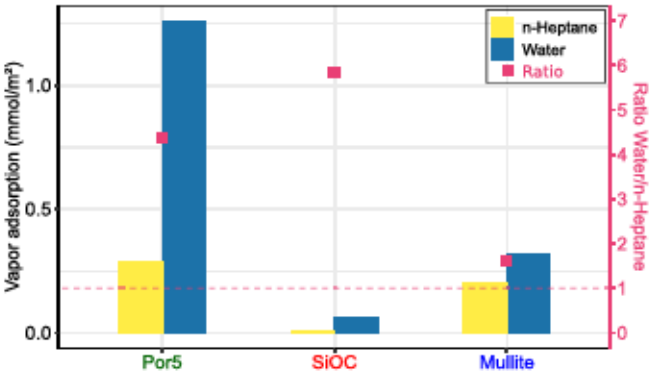

Fig. 4. Surface hydrophilicity-hydrophobicity measured by water and n-heptane vapor adsorption analysis of the membranes at 25 °C (the data correspondent to SiOC sample was extracted from Ref. [21]).

The water permeation flux through the membranes at a fixed transmembrane pressure of 5 bar is depicted in Fig. 5. As one may expect, due to the smaller membrane thickness (6.11 µm) the asymmetric membrane (mullite) shows the most expressive water permeation performance ($43 \times 10^{-3} \pm 6 \times 10^{-3}$ m^3 m^{-2} s^{-1}). The asymmetric morphology minimizes the hydraulic resistance, hence resulting in higher flux against symmetric structures [27]. Concerning the symmetric membranes, the SiOC ($7 \times 10^{-3} \pm 1 \times 10^{-3}$ m^3 m^{-2} s^{-1}) presents almost two times the performance of Por5 ($3.8 \times 10^{-3} \pm 0.3 \times 10^{-3}$ m^3 m^{-2} s^{-1}). These values corroborate that the pore diameter, pore size

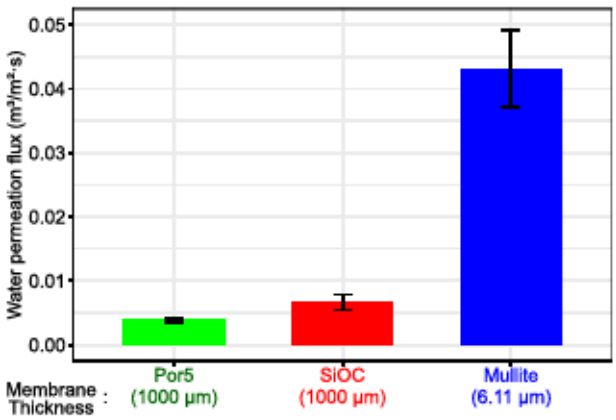

Fig. 5. Water permeation flux of the membranes at a constant pressure of 5 bar and at 25 °C (the data correspondent to Por5 and Mullite were extracted from Ref. [20]).

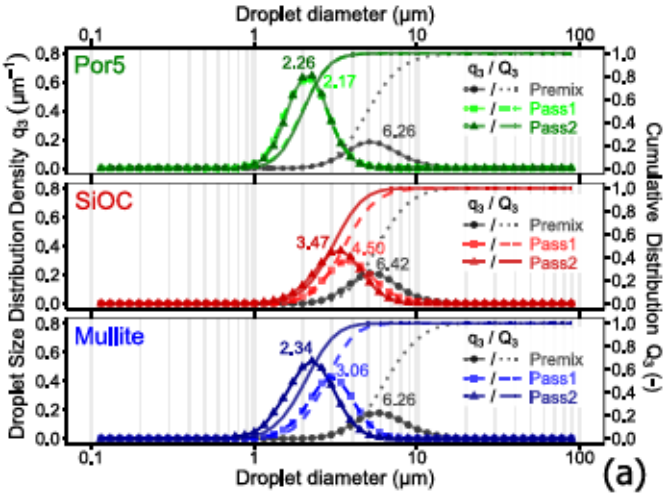

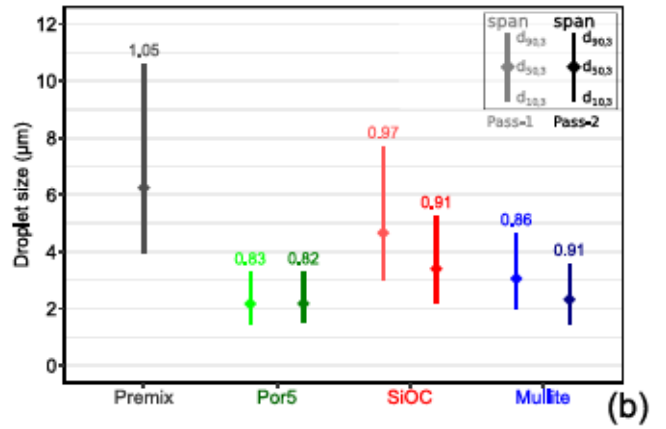

Fig. 6. (a) Droplet size distribution obtained from premix emulsification of oil-in-water emulsion (Premix = 10 wt% MCT + 1 wt% polysorbate 80) at 5 bar for the studied inorganic membranes (values above the curves indicate the mean droplet size given by the median diameter in µm – $d_{50,3}$). (b) Span values and characteristics sizes in terms of $d_{10,3}$, $d_{50,3}$ and $d_{90,3}$ according to the membrane and number of passes at 5 bar.

distribution, and morphology (asymmetry or symmetry) are the major parameters that affect the water flow through the membrane. However, the open porosity in the symmetric membranes appears to have no major

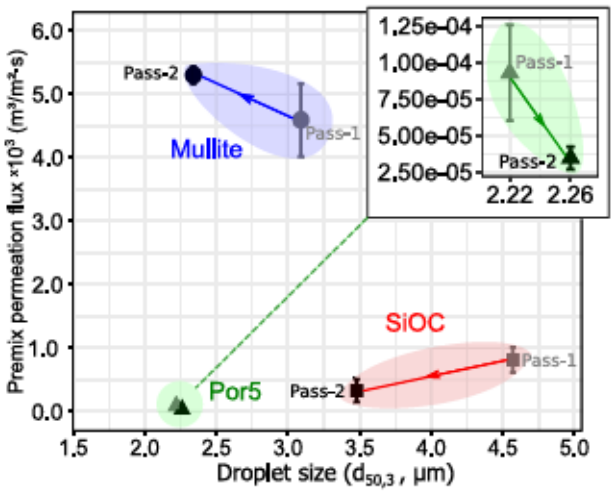

Fig. 7. Premix permeation flux ($m^3\ m^{-2}\ s^{-1}$) at 5 bar as a function of the median droplet size ($d_{50,3}$, µm) and the number of passes for the studied membranes.

effect on the permeation properties. The higher hydrophilic behavior of SiOC (ratio = 5.84) compared to Por5 (ratio = 4.37) may have a contribution to its slight superior water flux. Nonetheless, it is not possible to clearly quantify its effect on the water permeation flux.

3.2. *Premix emulsification using different ceramic membranes*

Fig. 6a shows the droplet size distribution curves and the cumulative curves of the prepared premix and the fine emulsions after one and two passes through the ceramic membranes at 5 bar. The mean droplet sizes (in terms of the median diameter $d_{50,3}$) are also given as indicated by the numbers above the curves. The fluctuation in the characteristic sizes ($d_{10,3}$, $d_{50,3}$, $d_{90,3}$) and span values based on each sample and pass are displayed in Fig. 6b. All the studied ceramic membranes display a tendency to generate a monomodal distribution (span < 1.0). Por5 seems to be insensitive to the number of passes, producing similar outputs in terms of $d_{50,3}$ and span values after Pass-1 (2.17 µm; 0.82) and Pass-2 (2.26 µm; 0.82). SiOC and mullite membranes demonstrate a major advantage in terms of practical application over the commercial Por5 concerning tailoring of the droplet size. Both membranes show an expected tendency of droplet size reduction due to the number of passes. The mean droplet sizes obtained from SiOC membrane varied from 4.5 µm (Pass 1) to 3.5 µm (Pass 2), with span values around 0.9. Mullite membrane produced $d_{50,3}$–span values in the range of 3.1 µm–0.9 (Pass 1) and 2.3 µm–0.9 (Pass 2). The results from the mullite membrane after Pass 2 are comparable to the ones from Por5. Generally, in premix membrane emulsification, thicker membranes generate more uniform emulsions due to multiple break-up points inside the membrane [11]. Nevertheless, in our work, the asymmetric structure produces a monomodal tendency analogous to the studied symmetric commercial membrane (Por5).

Comparatively, a study reported the preparation of stable oil-in-water emulsions (10 vol% sunflower oil fraction, and 2 wt% polysorbate 20) using flat commercial nitrocellulose mixed ester (MCE) membranes (0.8 µm pore size) [5]. Although the authors show a reduction of the mean droplet diameter (d_{32}) from ~5 µm (premix) up to ~2 µm after one pass at 5 bar (flux ~6.9×10^{-3} $m^3\ m^{-2}\ s^{-1}$), the size distribution exhibited two main peaks at 1 and 10 µm. A monomodal tendency was obtained only after the third pass (flux ~9.2×10^{-3} $m^3\ m^{-2}\ s^{-1}$) where the mean droplet size was around 1.24 µm with a span value of 0.82. Despite some similarities with our work, there is a fundamental point that differentiates our membrane from this mentioned study, which is the structural stability inherent from ceramic

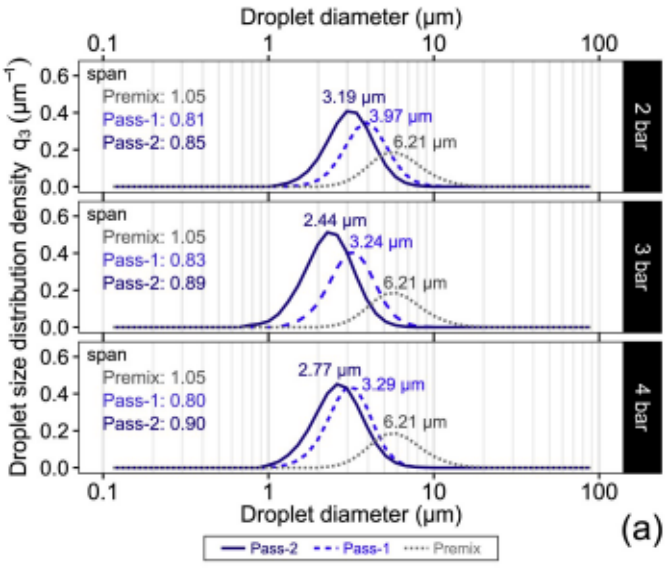

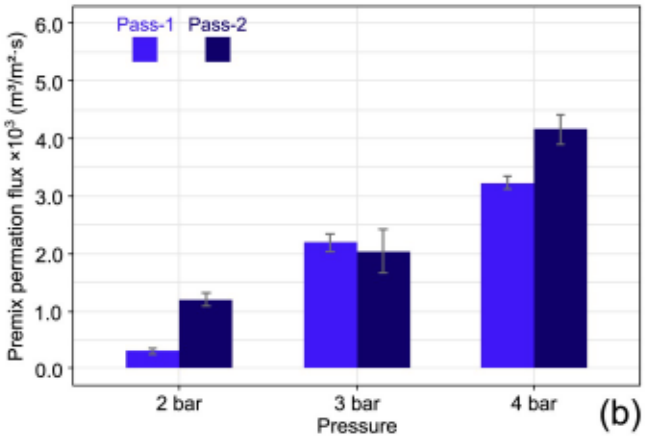

Fig. 8. (a) Droplet size distribution density (μm^{-1}) and span values obtained from the premix membrane emulsification experiment of oil-in-water emulsion (MCT 10 wt%) at different pressures (2, 3, and 4 bar) and 2 passes through the mullite asymmetric membrane (the values above the curves represent the $d_{50,3}$). (b) Premix permeation flux ($m^3\ m^{-2}\ s^{-1}$) as a function of the applied pressure and number of passes for the mullite membrane.

materials. Since the mentioned work deals with organic microfiltration membranes, changes in the membrane surface structure and thickness were observed, which can drastically reduce reproducibility, efficiency, and lifespan.

The relationship between mean droplet size and permeation flux at 5 bar according to the number of passes is given in Fig. 7. Although mullite and Por5 membranes have similar emulsification performance regarding droplet size and span values; Fig. 7 reveals that mullite is much more suitable for upscaling given their permeation fluxes ($4.6 \times 10^{-3} - 5.3 \times 10^{-3}$ $m^3\ m^{-2}\ s^{-1}$, Pass-1 and Pass-2, respectively). The symmetric membranes show inferior premix permeation fluxes, falling in a range below 1×10^{-3} $m^3\ m^{-2}\ s^{-1}$. Another interesting observation concerns the lower flux during the second pass (Pass-2) for the symmetric membranes, suggesting problems related to fouling. Even though the SiOC membrane displays a reduction in flux, it also results in a steep decrease in mean droplet size. Conversely, Por5 results suggest that this membrane is already operating in a threshold zone, in which there is a minor drop in flux and mean droplet size. However, the asymmetric mullite membrane displays a reduction in droplet size from Pass 1 to Pass 2 accompanied by an increment in the premix permeation flux. Since the primary droplet disruption and size reduction occur during the first pass,

Table 2
Premix emulsification studies of oil-in-water emulsions using different ceramic membranes in a dead-end configuration.

Membrane characteristics	Premix (O/W)		Droplet characteristics after PME		PME parameters		Ref.
	Composition	Characteristics	Size (μm)	span	*P* (bar)	*J* ($m^3/m^2 \cdot s$)	
Por5 (Robuglas) borosilicate glass; flat disc; symmetric structure $d_m = 1.39$ μm; $\varepsilon = 77.83\%$	MCT oil [10 wt%] Polysorbate 80 [1 wt%] (~25 °C)	$d_{50,3} = 6.26$ μm span = 1.05 ~25 °C	$d_{50,3(Pass1)} = 2.17$ $d_{50,3(Pass2)} = 2.26$	Pass1 = 0.83 Pass2 = 0.82	5	Pass1 = 9.3×10^{-5} Pass2 = 3.5×10^{-5}	This work
SiOC flat disc membrane; symmetric structure $d_m = 1.76$ μm; $\varepsilon = 36.45\%$	MCT oil [10 wt%] Polysorbate80 [1 wt%] (~25 °C)	$d_{50,3} = 6.42$ μm span = 1.05 ~25 °C	$d_{50,3(Pass1)} = 4.50$ $d_{50,3(Pass2)} = 3.47$	Pass1 = 0.97 Pass2 = 0.91	5	Pass1 = 8.2×10^{-4} Pass2 = 3.3×10^{-4}	This work
Mullite flat disc membrane; asymmetric structure; $d_m = 3.06$ μm; $\varepsilon = 68.27\%$ $d_{m(top)}E = 1.18 \pm 0.8$ μm	MCT oil [10 wt%] Polysorbate80 [1 wt%]	$d_{50,3} = 6.26$ μm span = 1.05 ~25 °C	$d_{50,3(Pass1)} = 3.97$–3.06 $d_{50,3(Pass2)} = 3.19$–2.34	Pass1 = 0.81–0.86 Pass2 = 0.85–0.91	2–5	Pass1 = $(0.3–4.6) \times 10^{-3}$ Pass2 = $(1.2–5.3) \times 10^{-3}$	This work
Glass membrane; Tubular shape; symmetric structure $d_{mA} = 2.70$ μm $d_{mB} = 4.20$ μm	Corn oil [25 wt%] PGPR [0.5 wt%] and PGFE [0.75–3.0 wt%]	$d_{50} = \sim 10$ μm 25 °C	$d_{32(A)} = 4.70$–5.72 $d_{32(B)} = 6.07$–8.72	A = 0.40–0.65 B = 0.62–0.66	A = 0.4–1.0 B = 0.1–0.6	A = $(8.1–197) \times 10^{-6}$ B = $(20–986) \times 10^{-6}$	[32]
α-Al_2O_3; Tubular shape; symmetric structure $d_m = 1.5$ μm	Toluene SDS [2 wt%]	$d_{50} = 54.69$ μm 20 °C	$d_{50} = 2.29$	1.2	2	1.26×10^{-4}	[33]
Shirasu Porous Glass; Tubular shape; symmetric structure $d_m = 8.0$ μm	Corn oil [40 wt%] SDS [0.06–2 wt%] or Polysorbate 20 [0.1–2 wt%]	$d_m = 119$ μm range = 10–204 μm 25 °C	$d_{m(Twenn-Pass5)} = 6.4$–8.7 $d_{m(SDS-Pass5)} = 4.1$–6.8	n.a.	1	Tween = $(1.4–13) \times 10^{-3}$ SDS = $(8.1–17) \times 10^{-3}$	[34]
Shirasu Porous Glass; Tubular shape; symmetric structure $d_m = 8.0$ μm	Corn oil [10 or 20 wt%] Lecithin [2 wt %]	$d_{m\ 10} = \sim 90$ μm $d_{m\ 20} = \sim 300$ μm 20 °C	$50\ \mu m < d_m < d_{Premix}$	n.a.	1 or 1.5	$(2.8–83) \times 10^{-4}$	[13]
Por2/3/4 (Robuglas) borosilicate glass; symmetric structure $d_{50} = 13/28/70$ μm; $\varepsilon = 42/41/36\%$; alumina/silica membranes; $d_{50} = 130$–314 μm; $\varepsilon = 34$–40%; Flat discs	Rapeseed oil [0.5 v/v] Tween 20 or Tween 80	$d_{32} = \sim 80$–170 μm span = 0.99–1.23	$d_{32} = 9$–29 μm	1.471–1.807	0.5–5	~120 (highest disperse phase flux rate)	[35]
Shirasu Porous Glass; Tubular shape; symmetric structure $d_m = 0.2$–0.8 μm	Ethylhexyl palmitate (EHP) [5–40 wt%] polysorbate 20 or 80 [2.5–20 wt%]	$d_{50} = \tilde{}15$ μm	$d_{50} = 0.26$–1.0	0.41–0.48	10–60	5–200 $mL \cdot min^{-1}$	[36]

ε – Porosity (%); PGPR – Polyglycerol polyricinoleate (CR-500: Hexaglycerol ester); PGFE – Polyglycerol fatty acid esters (Decaglycerol monolaurate; HLB: 10–15); SDS – Sodium dodecyl sulfate; n.a. – not available.

an intensification in flux may be expected in the second pass [11]. This behavior might be true for the asymmetric membrane due to its lower susceptibility to fouling as compared to the other membranes.

3.3. Premix emulsification using mullite membrane at lower pressures

Considering its premix permeation flux and the resultant droplet size, the mullite membrane was further studied under lower transmembrane pressures (2–4 bar). Generally, asymmetric membranes tend to outperform when compared to symmetric structures since there is less hindrance in the permeation flux owing to the reduced selective layer thickness. In asymmetric membranes, structural as well as transport properties vary over the cross section of the membrane and its perme-ation characteristics are determined by the nature of the material or the size of pores in the skin layer [28]. Fig. 8a and Fig. 8b portray, respec-tively, the droplet diameter distribution (μm) and the premix perme-ation flux ($m^3\ m^{-2}\ s^{-1}$) of the prepared emulsions as a function of the number of passes and the applied pressure. From Fig. 8a, it is possible to observe that the droplet diameter is inversely proportional to the applied pressure and number of passes. Nevertheless, the reduction of the droplet size does not appear to follow a linear relationship. For instance, taking into consideration the Pass 1, the premix was reduced from 6.21 μm to 3.97 μm (2 bar), 3.24 μm (3 bar), and 3.29 μm (4 bar). Moreover, the span values of the produced emulsions are quite similar; however, it seems to have a trend of slight broadening of the size dis-tribution after the second pass through the membrane (span: Pass 1 < Pass 2). This increment in span after the second pass is most probably a result of the combination of break-up and coalescence that ultimately increase slightly the size distribution as the number of passes progress [7]. With respect to the premix permeation flux (Fig. 8b), an increment with the transmembrane pressure is observed. Nonetheless, as one may expect, compared to pure water flux, there is a clear decrease in the premix flux due to the presence of a viscous dispersed component (oil phase) [29,30]. In addition, as observed in Fig. 7 at 5 bar, during Pass 2 the permeation flux presented a substantial increase at 2 and 4 bar. Even though, at 3 bar the mean flux value of Pass 2 ($2.0 \times 10^{-3} \pm 0.4 \times 10^{-3}$ $m^3\ m^{-2}\ s^{-1}$) is marginally inferior to Pass 1 ($2.2 \times 10^{-3} \pm 0.1 \times 10^{-3}$ $m^3\ m^{-2}\ s^{-1}$), the superior limit of the error bar in Pass 2 overpasses the one in Pass 1. A reduction in droplet size with multiple passings has been reported in Refs. [11]. The observed reduction in droplet size due to the applied pressure (Fig. 8a) can be described as an effect of the direct relationship between pressure and permeating flux (as stated in Darcy's law) [31].

Table 2 summarizes the main parameters and outcomes concerning the premix emulsification process in a dead-end configuration using ceramic membranes. The results of our work are compared to the main studies from the literature. It is noteworthy that our membranes are quite competitive, particularly the asymmetric mullite membrane due to its flux performance. For instance, the flat mullite membrane from this work presents characteristics similar to the work described by Jing et al. [33]. Nevertheless, the flux output from the asymmetric mullite membrane at Pass-2 ($1.2 \times 10^{-3}\ m^3\ m^{-2}\ s^{-1}$) is 10 times higher ($1.26 \times 10^{-4}$ $m^3\ m^{-2}\ s^{-1}$) at the same applied pressure (2 bar) [33]. Moreover, most of the studies presented in Table 2 are related to tubular membranes, which are still the most usual in the current market of inorganic membranes. This fact is probably related to the more uniform pressure distribution in cylindrical shapes when compared to flat ones, which may reduce breakage due to differential stress spots in the structure. In addition, the works presented in Table 2 are all related to inorganic membranes with symmetric structures.

4. Conclusions

The preparation of a stable oil-in-water emulsion is investigated by using the PME process with three distinct microfiltration inorganic membranes. The effect of the number of passes on the mean droplet size and the dispersity (span) is demonstrated. All membranes produced a mono-modal droplet size distributions (span < 1). The commercial symmetric Por5 is the only membrane insensitive to the number of passes. The symmetric SiOC and the asymmetric mullite membranes exhibit a decrease in droplet size after a second pass through the membrane. The droplet size and the span values obtained for the manufactured mullite membrane is comparable to the commercial Por5. However, the asymmetric structure of the mullite membrane shows a superior flux performance against to the symmetric membranes. Therefore, the results obtained in this work corroborate the potential application of ceramic membranes in the ME process, particularly the one with asymmetric structure.

Declaration of competing interest

The authors declare that they have no known competing financial interests or personal relationships that could have appeared to influence the work reported in this paper.

Acknowledgements

We thank the German Research Foundation (DFG) within the Research Training Group GRK 1860 "Micro-, meso- and macroporous nonmetallic Materials: Fundamentals and Applications" (MIMENIMA). We are grateful to the funding agencies Coordination for the Improvement of Higher Education Personnel (CAPES, Brazil) in partnership with DFG through the Brazilian-German Collaborative Research Initiative on Manufacturing (BRAGECRIM; process number 88887.143922/2017–00 and WI 3131/5-1), and the National Council for Scientific and Technological Development (CNPq, Brazil; process number 142148/2015-6) for supporting this study. Natália Cristina Fontão and Bernardo Araldi da Silva are also acknowledged for the vapor adsorption analysis and BET specific surface area measurement of the Por5 membrane, respectively.

Appendix A. Supplementary data

Supplementary data to this article can be found online at https://doi.org/10.1016/j.memsci.2020.118124.

References

[1] D.J. Shaw, Introduction to Colloid and Surface Chemistry, Butterworth-Heinemann, 1992.
[2] S.M. Joscelyne, G. Trägårdh, Membrane emulsification — a literature review, J. Membr. Sci. 169 (1) (2000) 107–117.
[3] C. Charcosset, I. Limayem, H. Fessi, The membrane emulsification process - a review, J. Chem. Technol. Biotechnol. 79 (3) (2004) 209–218, https://doi.org/10.1002/jctb.969.
[4] A. Trentin, M. Ferrando, F. López, C. Güell, Premix membrane O/W emulsification: effect of fouling when using BSA as emulsifier, Desalination 245 (1–3) (2009) 388–395, https://doi.org/10.1016/j.desal.2009.02.002.
[5] A. Trentin, C. Güell, F. López, M. Ferrando, Microfiltration membranes to produce BSA-stabilized O/W emulsions by premix membrane emulsification, J. Membr. Sci. 356 (1–2) (2010) 22–32, https://doi.org/10.1016/j.memsci.2010.03.022.
[6] L. Giorno, G. De Luca, A. Figoli, E. Piacentini, E. Drioli, Membrane emulsification: principles and applications, in: E. Drioli, L. Giorno (Eds.), Membr. Oper. Innov. Sep. Transform., Wiley-VCH Verlag GmbH & Co. KGaA, 2009, pp. 463–497, https://doi.org/10.1002/9783527626779.ch21. Ch. 21.
[7] A. Nazir, R.M. Boom, K. Schroën, Droplet break-up mechanism in premix emulsification using packed beds, Chem. Eng. Sci. 92 (2013) 190–197, https://doi.org/10.1016/j.ces.2013.01.021.
[8] E. Piacentini, E. Drioli, L. Giorno, Membrane emulsification technology: twenty-five years of inventions and research through patent survey, J. Membr. Sci. 468 (2014) 410–422, https://doi.org/10.1016/j.memsci.2014.05.059.
[9] H.S. Ribeiro, J.J.M. Janssen, I. Kobayashi, M. Nakajima, Klaus-Viktor Peinemann, S.P. Nunes, L. Giorno, Membrane emulsification for food applications, in: Membr. Technol. 3 Membr. Food Appl., vol. 3, Wiley-VCH Verlag GmbH & Co. KGaA, 2010, pp. 129–166, https://doi.org/10.1002/9783527631384.ch7. Ch. 7.
[10] V. Zanatta, K. Rezzadori, F. Marques, G. Zin, C. Cunha, M. Di Luccio, E. Lemos-Senna, Stability of oil-in-water emulsions produced by membrane emulsification with microporous ceramic membranes, J. Food Eng. 195 (2017) 73–84, https://doi.org/10.1016/j.jfoodeng.2016.09.025.

[11] A. Nazir, K. Schroën, R. Boom, Premix emulsification: a review, J. Membr. Sci. 362 (1–2) (2010) 1–11, https://doi.org/10.1016/j.memsci.2010.06.044.
[12] G.T. Vladisavljević, M. Shimizu, T. Nakashima, Preparation of monodisperse multiple emulsions at high production rates by multi-stage premix membrane emulsification, J. Membr. Sci. 244 (1–2) (2004) 97–106, https://doi.org/10.1016/j.memsci.2004.07.008.
[13] J. Surh, Y.G. Jeong, G.T. Vladisavljević, On the preparation of lecithin-stabilized oil-in-water emulsions by multi-stage premix membrane emulsification, J. Food Eng. 89 (2) (2008) 164–170, https://doi.org/10.1016/j.jfoodeng.2008.04.023.
[14] D. da Silva Biron, V. dos Santos, M. Zeni, Ceramic Membranes Applied in Separation Processes, 2018, https://doi.org/10.1007/978-3-319-58604-5. http://link.springer.com/10.1007/978-3-319-58604-5.
[15] M. Matos, M.A. Suárez, G. Gutiérrez, J. Coca, C. Pazos, Emulsification with microfiltration ceramic membranes: a different approach to droplet formation mechanism, J. Membr. Sci. 444 (2013) 345–358, https://doi.org/10.1016/j.memsci.2013.05.033.
[16] F. Spyropoulos, D.M. Lloyd, R.D. Hancocks, A.K. Pawlik, Advances in membrane emulsification. Part A: recent developments in processing aspects and microstructural design approaches, J. Sci. Food Agric. 94 (4) (2014) 613–627, https://doi.org/10.1002/jsfa.6444.
[17] L. Luhede, T. Wollborn, U. Fritsching, Stability of multiple emulsions under shear stress, Can. J. Chem. Eng. 98 (1) (2019), https://doi.org/10.1002/cjce.23578. https://onlinelibrary.wiley.com/doi/pdf/10.1002/cjce.23578.
[18] Iso4793, Laboratory sintered (fritted) filters - porosity grading, classification and designation, Int. Organ. Stand. 1 (1980) 1–7. https://www.iso.org/standard/10772.html.
[19] Robu® Glasfilter-Geräte GmbH, Porengrössen. https://www.robuglas.com/index.php?id=51{&}L=1.
[20] R.K. Nishihora, E. Rudolph, M.G.N. Quadri, D. Hotza, K. Rezwan, M. Wilhelm, Asymmetric mullite membranes manufactured by phase-inversion tape casting from polymethylsiloxane and aluminum diacetate, J. Membr. Sci. 581 (2019) 421–429, https://doi.org/10.1016/j.memsci.2019.03.047. https://linkinghub.elsevier.com/retrieve/pii/S0376738818335208.
[21] R.K. Nishihora, M.G.N. Quadri, D. Hotza, K. Rezwan, M. Wilhelm, Tape casting of polysiloxane-derived ceramic with controlled porosity and surface properties, J. Eur. Ceram. Soc. 38 (15) (2018) 4899–4905, https://doi.org/10.1016/j.jeurceramsoc.2018.07.016.
[22] H. Zhang, P. D'Angelo Nunes, M. Wilhelm, K. Rezwan, Hierarchically ordered micro/meso/macroporous polymer-derived ceramic monoliths fabricated by freeze-casting, J. Eur. Ceram. Soc. 36 (1) (2016) 51–58, https://doi.org/10.1016/j.jeurceramsoc.2015.09.018.
[23] V. Kozák, Z. Sucharda, M. Havelcová, I. Dlouhý, P. Glogar, Z. Chlup, M. Černý, A. Strachota, Preparation of Silicon Oxycarbide composites toughened by inorganic fibers via pyrolysis of precursor siloxane composites, Acta Phys. Pol., A 120 (2) (2016) 326–330, https://doi.org/10.12693/aphyspola.120.326.
[24] J. Kujawa, W. Kujawski, Functionalization of ceramic metal oxide powders and ceramic membranes by perfluoroalkylsilanes and alkylsilanes possessing different reactive groups: physicochemical and tribological properties, ACS Appl. Mater. Interfaces 8 (11) (2016) 7509–7521, https://doi.org/10.1021/acsami.5b11975.
[25] J. Li, K. Lu, T. Lin, F. Shen, Preparation of micro-/mesoporous SiOC bulk ceramics, J. Am. Ceram. Soc. 98 (6) (2015) 1753–1761, https://doi.org/10.1111/jace.13541.
[26] J. Li, K. Lu, Highly porous SiOC bulk ceramics with water vapor assisted pyrolysis, J. Am. Ceram. Soc. 98 (8) (2015) 2357–2365, https://doi.org/10.1111/jace.13634.
[27] A.J. Burggraaf, Chapter 2 Important characteristics of inorganic membranes, Membr. Sci. Technol. 4 (C) (1996) 21–34, https://doi.org/10.1016/S0927-5193(96)80005-2.
[28] H. Strathmann, L. Giorno, E. Drioli, 1.05 - basic aspects in polymeric membrane preparation*, in: E. Drioli, L. Giorno (Eds.), Comprehensive Membrane Science and Engineering, Elsevier, Oxford, 2010, pp. 91–112, https://doi.org/10.1016/B978-0-08-093250-7.00057-8. http://www.sciencedirect.com/science/article/pii/B9780080932507000578.
[29] O. Alliod, L. Messager, H. Fessi, D. Dupin, C. Charcosset, Influence of viscosity for oil-in-water and water-in-oil nanoemulsions production by SPG premix membrane emulsification, Chem. Eng. Res. Des. 142 (2018) 87–99, https://doi.org/10.1016/j.cherd.2018.11.027. https://linkinghub.elsevier.com/retrieve/pii/S0263876218306075.
[30] G.T. Vladisavljević, U. Lambrich, M. Nakajima, H. Schubert, Production of O/W emulsions using SPG membranes, ceramic α-aluminium oxide membranes, microfluidizer and a silicon microchannel plate - a comparative study, Colloids Surfaces A Physicochem. Eng. Asp. 232 (2–3) (2004) 199–207, https://doi.org/10.1016/j.colsurfa.2003.10.026.
[31] N. Li, K. Sakaki, Performance of an emulsion enzyme membrane reactor combined with premix membrane emulsification for lipase-catalyzed resolution of enantiomers, J. Membr. Sci. 314 (1–2) (2008) 183–192, https://doi.org/10.1016/j.memsci.2008.01.052.
[32] I.S. Kanichi Suzuki, Y. Hagur, Characteristics of the membrane emulsification method combined with preliminary emulsification for preparing corn oil-in-water emulsions, Food Sci. Technol. 2 (1) (1996) 43–47, https://doi.org/10.3136/fsti9596t9798.2.43.
[33] W. Jing, J. Wu, W. Xing, W. Jin, N. Xu, Emulsions prepared by two-stage ceramic membrane jet-flow emulsification, Part, Technol. Fluid. 51 (5) (2005) 1339–1345, https://doi.org/10.1002/aic.10405.
[34] G.T. Vladisavljevic, J. Surh, J.D. Mcclements, Effect of emulsifier type on droplet disruption in repeated Shirasu Porous Glass membrane homogenization, Langmuir 22 (10) (2006) 4526–4533, https://doi.org/10.1021/la053410f.
[35] N. Hornig, U. Fritsching, Liquid dispersion in premix emulsification within porous membrane structures, J. Membr. Sci. 514 (2016) 574–585, https://doi.org/10.1016/j.memsci.2016.04.051.
[36] O. Alliod, J.-p. Valour, S. Urbaniak, H. Fessi, D. Dupin, C. Charcosset, Preparation of oil-in-water nanoemulsions at large-scale using premix membrane emulsification and Shirasu Porous Glass (SPG) membranes, Colloids Surf., A 557 (April) (2018) 76–84, https://doi.org/10.1016/j.colsurfa.2018.04.045.